A mmWave Full-Duplex MIMO Antenna With EBG-Based Self-Interference Suppression

Hadi Hosseini, Adewale K. Oladeinde, and Ehsan Aryafar
Portland State University, Portland, OR, USA

***Abstract*—Full-duplex (FD) mmWave communication has the potential to significantly increase spectral efficiency by enabling simultaneous transmission and reception. A primary challenge in realizing FD operation is strong self-interference (SI) caused by coupling between co-located transmit and receive antennas, particularly in compact MIMO arrays. In this work, we address SI suppression at the antenna level through a novel high-impedance stacked electromagnetic band-gap (HIS-nSEBG) structure integrated into a 1×4 transmit–receive MIMO antenna array operating in the 28 GHz band. The proposed EBG consists of vertically stacked metallic patch layers embedded within a four-layer antenna stack-up to maximize coupling suppression without degrading radiation performance. The antenna array is designed and optimized using full-wave HFSS simulations and subsequently fabricated and experimentally characterized. Extensive evaluations show that (i) port-to-port isolation obtained from vector network analyzer measurements closely follows full-wave HFSS simulations; (ii) the proposed HIS-nSEBG provides an average isolation improvement of 25 dB over a 1.4 GHz bandwidth compared to a baseline MIMO antenna without EBGs; and (iii) the operating bandwidth and antenna gain are not negatively impacted by the EBG integration.**

***Index Terms*—Full-duplex MIMO wireless, MmWave bands, Electromagnetic band gap, Stacked patch antennas**

I. Introduction

The growing demand for high-data-rate wireless services, combined with limited spectrum availability in sub-6 GHz bands, has accelerated the adoption of millimeter-wave (mmWave) technologies for 5G and beyond. The Ka-band (26.5–40 GHz), in particular, is being used to provide large contiguous bandwidths that support multi-gigabit data rates for emerging technologies and applications such as augmented and virtual reality (AR/VR), AI-driven autonomous systems, and dense cellular deployments [1], [2]. In the United States, for example, Verizon holds a significant portion of the 28 GHz spectrum and exploits wideband channels to increase network capacity. On a parallel front, full-duplex (FD) wireless has emerged as a promising technique to improve spectral efficiency by allowing simultaneous transmission and reception on the same frequency channel. The key limitation of FD operation is self-interference (SI), where the strong transmit signal couples into the co-located receive chain and causes a significant amount of SI on the receiving antenna [1], [3].

Antenna-level isolation techniques are particularly attractive for mitigating SI at mmWave frequencies, as they suppress interference before it reaches the RF front-end. In practice, FD wireless systems combine such passive suppression with analog and/or digital cancellation to further reduce the remaining SI [3].

An electromagnetic band-gap (EBG) structure suppresses electromagnetic wave propagation over a specific frequency range, effectively preventing radio waves from traveling through the medium. EBG structures have been widely explored as an effective means of suppressing mutual coupling in antenna arrays across both mmWave and Sub-6 GHz frequency bands [4], [5], [6], [7]. In our prior work [8], we introduced a novel high-impedance stacked electromagnetic band-gap (HIS-nSEBG) structure and demonstrated significant SI reduction for a single transmit–receive mmWave FD antenna operating at 28 GHz. The proposed SI mitigation is achieved through a stacked EBG configuration that forms a high-impedance barrier to surface and near-field electromagnetic wave propagation between the transmit (Tx) and receive (Rx) antenna elements. In this paper, we extend that design to a MIMO antenna array. In FD MIMO architectures, multiple simultaneously active transmit and receive antennas introduce additional coupling paths, making isolation enhancement increasingly difficult as array size increases. The key contributions of this work are summarized as follows:

- **Design and Prototype:** We design a FD mmWave MIMO antenna architecture comprising two separate 1×4 transmit and receive antenna arrays integrated on the same PCB design. The HIS-nSEBG structure [8] is embedded between the transmit and receive elements to suppress SI. Full-wave simulations using Ansys HFSS are performed to optimize the return loss, radiation characteristics, and port-to-port isolation, and a multilayer prototype is fabricated for practical RF characterization.
- **Evaluation:** The proposed MIMO antenna array is experimentally characterized using a two-port vector network analyzer, where isolation measurements are performed sequentially between a single active transmit antenna and multiple receive antennas at varying spatial separations. Measured results show good agreement with HFSS simulations and demonstrate approximately 25 dB additional isolation over a wide bandwidth compared to a baseline MIMO antenna without EBGs. The results further confirm that isolation improves with increased transmit–receive separation, validating the scalability of the HIS-nSEBG approach for full-duplex mmWave MIMO systems.

The rest of this paper is organized as follows. Section II describes the proposed antenna and HIS-nSEBG design. Section III presents the results of extensive simulations and measurements. Finally, Section IV concludes the paper.

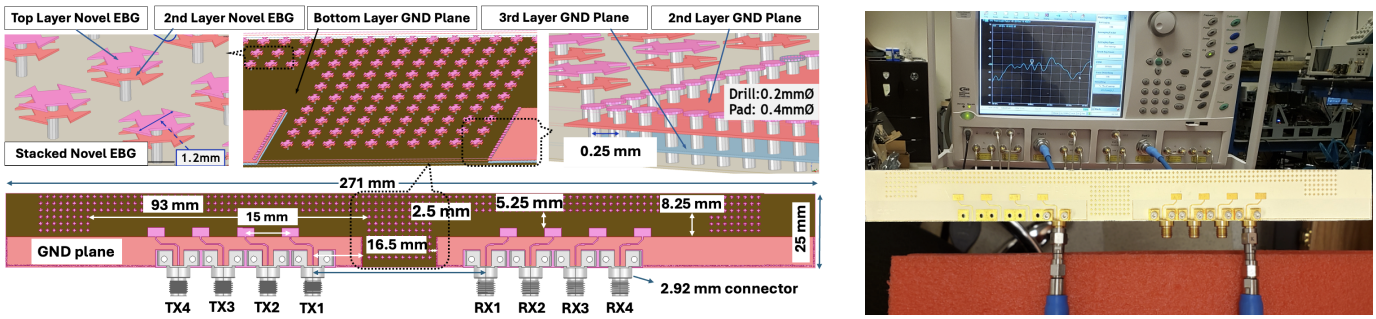

(a) (b)

Fig. 1: (a-bottom) Relative dimensions of the Tx and Rx array elements with respect to the HIS-nSEBG, (a-top left) four-layer stack-up structure with a zoomed-in 3D view of the HIS-nSEBG, highlighting the top and second-layer EBG patches, (a-top right) the PCB stitching vias around the EBG walls, (b) 2-port VNA measurement setup used to characterize fabricated antenna return loss and port-to-port isolation.

II. Antenna and HIS-nSEBG Design

A. Patch Antenna Design, and MIMO Integration

The antenna elements employed in the proposed MIMO array are rectangular microstrip patch antennas designed to operate in the Ka-band around 28 GHz. Microstrip patches are well suited for mmWave integration due to their low profile, planar form factor, and compatibility with multilayer PCB fabrication. The unit antenna element was previously designed and experimentally validated in our prior work [8].

As shown in Fig. 1(a-bottom), eight identical copies of the unit antenna element are arranged to form two separate 1×4 transmit and receive arrays on the same PCB design. The physical separation between the Tx and Rx arrays provides more than 30 dB of inherent SI reduction. In addition, the short wavelengths at mmWave frequencies enable dense antenna integration on a compact device, allowing spatial separation to be effectively exploited for further SI suppression.

The antenna stack-up consists of four layers. The top layer hosts the rectangular patch antenna elements and the pad interfaces for 2.92-mm RF connectors. The second layer (L2) serves as the ground reference plane for the antenna feeds, with a rectangular void introduced beneath each patch to enhance radiation efficiency. A similar void is incorporated in the third layer (L3) to further improve antenna performance. The bottom layer forms a solid ground reference plane and provides the mechanical support required for RF connector assembly. Each antenna element is excited through a 15-mm microstrip feed line and interfaced using a 50-Ω end-launch female 2.92-mm RF connector rated for operation up to 40 GHz.

The complete antenna system integrates the Tx and Rx arrays on a single multilayer PCB, with the HIS-nSEBG structure embedded in the inter-array region to suppress surface-wave and near-field coupling. Additional via stitching and guard rows are employed to mitigate fringing fields, and unwanted parallel plates resonances that could result in higher order mode and spurious emission. The array is fabricated using standard multilayer PCB manufacturing processes, ensuring accurate alignment of the stacked EBG layers and reliable via connections. End-launch connectors are soldered directly to the feed pads to minimize transition loss and measurement uncertainty at Ka-band frequencies, enabling repeatable experimental characterization.

B. HIS-nSEBG Design and Electromagnetic Operation

Self-interference (SI) between the Tx and Rx antenna arrays is mitigated using a novel high-impedance surface stacked electromagnetic band-gap (HIS-nSEBG) structure integrated into the antenna substrate. The proposed two-layer, mushroom-type stacked EBG [9] is embedded in the inter-array region to suppress port-to-port mutual coupling, enabling effective passive SI suppression in a mmWave FD radio.

Fig. 1(a-top) illustrates the HIS-nSEBG embedded within a four-layer antenna stack-up consisting of top, second, third, and bottom metal layers. The HIS-nSEBG comprises periodically arranged metallic patches implemented on two adjacent metal layers and connected to a common ground plane through metallized vias, forming a vertically stacked periodic surface. Compared to conventional single-layer mushroom EBG designs [10], [9], [11], the stacked configuration enhances coupling suppression while providing a wider electromagnetic stopband without increasing the lateral footprint.

Each HIS-nSEBG unit cell can be modeled as a parallel LC resonant circuit [8], where the via contributes an inductive component L and the overlapping stacked patches introduce an effective capacitance C . At resonance, the surface impedance becomes very high, suppressing surface-wave propagation and near-field coupling between adjacent antenna elements.

In the proposed layout, ten columns of HIS-nSEBG elements are positioned centrally between the Tx and Rx arrays, with the outermost columns placed 2.5 mm from the solid ground plane. To mitigate fringing field and preserve antenna gain, a peripheral guard ring is incorporated, consisting of three rows of HIS-nSEBG elements along the top edge and a 3×8 arrangement along the left and right edges, as shown in Fig. 1(a).

The dimensions and periodicity of the HIS-nSEBG are optimized using HFSS simulations to align the electromagnetic

bandgap with the antenna operating frequency while minimizing unwanted scattering and radiation pattern distortion.

III. Performance Evaluation

This section evaluates the performance of the proposed FD mmWave MIMO antenna through both full-wave simulations and experimental measurements. The return loss and port-to-port isolation between the transmit and receive array elements are first examined using Ansys HFSS and validated through vector network analyzer measurements. The impact of the HIS-nSEBG on antenna gain and radiation characteristics is then investigated through comparative HFSS simulations with and without the EBG structure. To measure and characterize the return loss and isolation of the fabricated antennas with/without the EBG structure, a 2-port Anritsu VNA measurement setup is used, as shown in Fig. 1(b).

Return Loss: Fig. 2(a) illustrates the simulated and lab-measured return loss ($|S_{11}|$) of the TX1 antenna element with and without EBG as a function of frequency. Using a -10 dB return-loss criterion, the measured bandwidth of the unit antenna is 1.4 GHz, spanning 27.4-28.8 GHz, which meets the bandwidth requirements for Gbps-rate mmWave communication at 28 GHz. The measured results show strong agreement with full-wave simulations; however, noticeable excursions exceeding 10 dB in some cases are observed near the lower and upper edges of the operating band. These could be partially attributed to the effect of PCB manufacturing tolerance that was not defined and modeled as part of original model simulation.

Isolation: Figs. 2(b) and 2(c) show the simulated and lab-measured port-to-port SI suppression between the TX1 antenna element and RX1–RX4 antenna elements with and without EBG, respectively. Both simulations and measurements indicate that, even without the EBG structure, up to 30 dB of SI reduction is achieved due to over-the-air path loss. The incorporation of the HIS-nSEBG provides an additional SI suppression of at least 25 dB over a 2.1 GHz bandwidth from 27.6 to 29.7 GHz.

To better understand the return loss of all antenna elements and the effect of the EBG on isolation between different Tx and Rx array elements, Fig. 3(a) shows the HFSS-simulated magnitude of the S-parameters $|S_{ij}|$ (dB) at 28 GHz for the baseline antenna without the EBG. Fig. 3(b) presents the corresponding results for the proposed design with the EBG, and Fig. 3(c) summarizes the resulting isolation improvement enabled by the EBG structure. A return loss of -10 dB or better is observed along the diagonal for all antenna elements. Although the EBG placement shows limited impact for some antenna element pairs at 28 GHz due to oscillatory coupling behavior across the bandwidth, the proposed design still achieves isolation levels of up to 80 dB. As expected, the closest Tx–Rx antenna pairs exhibit the lowest isolation, on the order of 60 dB, while the farthest receive antenna elements achieve higher isolation approaching 80 dB.

Figs. 3(d)-(f) present the average magnitude of the S-parameters $|S_{ij}|$ over the antenna operating bandwidth from 24.4 to 28.8 GHz. As shown in Figs. 3(d) and (e), the two antenna designs (i.e., with and without the EBG) exhibit average isolation levels of -15 dB or lower between different antenna elements. The impact of the EBG placement becomes more evident as illustrated in Fig. 3(f), where the proposed design achieves an average additional isolation improvement of approximately 25 dB due to the HIS-nSEBG structure over the operating band.

In the proposed MIMO antenna configuration, the analysis focuses on Tx–Rx self-interference, and cross-interference among Tx elements or among Rx elements is not considered. Nevertheless, the results show that isolation increases with inter-element spacing, which is primarily attributed to over-the-air path loss.

Far-field results: For all far-field evaluations in HFSS, the antenna is excited at port TX1, with all other ports terminated using 50-Ω matched loads. Fig. 4(a) and Fig. 4(b) show the simulated radiation patterns of the proposed MIMO antenna in the $\phi = 90^\circ$ (H-plane) and $\phi = 0^\circ$ (E-plane), respectively, at 28 GHz, including both co- and cross-polarized components for configurations with and without the EBG structure. In the H-plane, a relatively higher cross-polarization level is observed, which is attributed to the proximity of the feed network and connector to the radiating elements, leading to additional field perturbations and coupling effects. In contrast, the E-plane radiation pattern exhibits dominant co-polarized radiation with a clear boresight maximum and a null in the cross-polarized component, indicating efficient radiation in the intended direction. Importantly, a close correlation is observed between the radiation patterns of antenna models with and without the EBG, confirming that the HIS-nSEBG integration does not distort the far-field characteristics.

Fig. 4(c) compares the simulated peak gain versus frequency for antenna configurations with and without the EBG structure. The results show that the proposed design maintains stable gain performance, with less than 0.8 dBi variation over the 27–28.5 GHz band. This demonstrates that the HIS-nSEBG effectively enhances isolation without compromising antenna gain or radiation behavior in the MIMO configuration.

IV. Conclusion

We studied a mmWave FD MIMO antenna with a novel high-impedance stacked electromagnetic band-gap (HIS-nSEBG) structure for antenna-level SI suppression. The proposed design achieves an average isolation improvement of 25 dB over a 1.4 GHz bandwidth at 28 GHz, with measured results closely matching full-wave simulations. Importantly, the integration of the HIS-nSEBG preserves antenna bandwidth and gain, demonstrating its effectiveness for compact mmWave FD systems.

Acknowledgements

This research was supported in part by an NSF award (CNS-1942305).

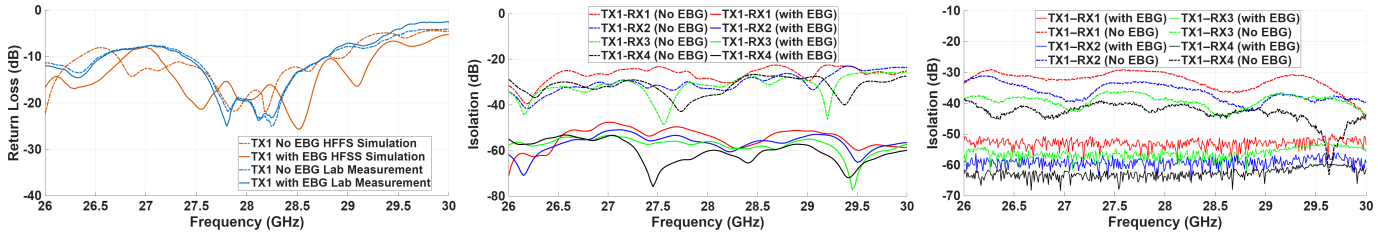

(a) (b) (c)

Fig. 2: (a) Simulated and lab-measured return loss ($|S_{11}|$) of the TX1 antenna element with and without EBG, (b) simulated port-to-port isolation between the TX1 antenna element and RX1–RX4 antenna elements with and without EBG, and (c) lab-measured port-to-port isolation between the TX1 antenna element and RX1–RX4 antenna elements with and without EBG.

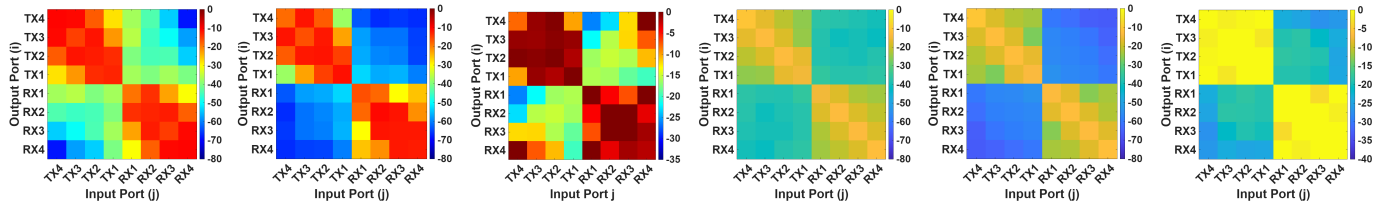

(a) (b) (c) (d) (e) (f)

Fig. 3: (a) HFSS-simulated magnitude of the S-parameters $|S_{ij}|$ (dB) at 28 GHz without the EBG structure, (b) magnitude of the S-parameters $|S_{ij}|$ (dB) at 28 GHz with the EBG structure, (c) isolation improvement (dB) due to the EBG structure, (d) average S-parameter magnitude $\overline{|S_{ij}|}$ (dB) over the antenna bandwidth (24.4–28.8 GHz) without the EBG structure, (e) average S-parameter magnitude $\overline{|S_{ij}|}$ (dB) over the antenna bandwidth with the EBG structure, and (f) average isolation improvement (dB) over the antenna bandwidth due to the EBG structure.

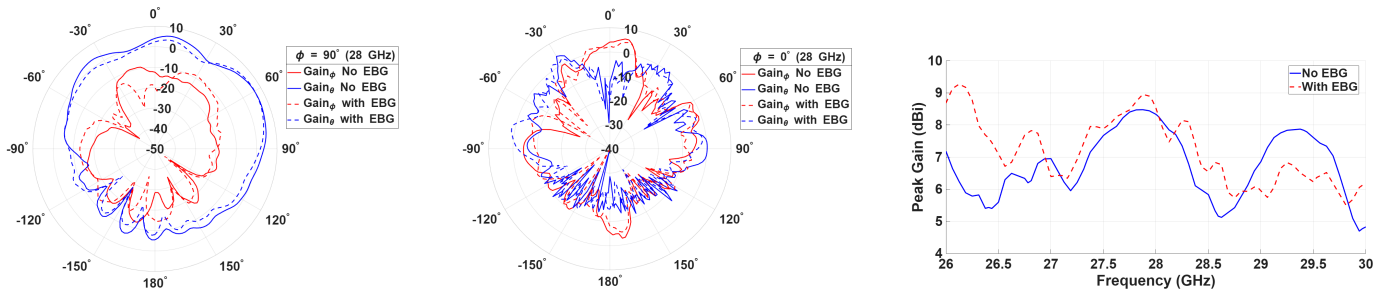

(a) (b) (c)

Fig. 4: (a) Simulated radiation patterns (dBi) in the $\phi = 90^\circ$ plane (H-plane) at 28 GHz showing co- and cross-polarized gain components for antenna models with and without EBG, (b) Simulated radiation patterns (dBi) in the $\phi = 0^\circ$ plane (E-plane) at 28 GHz showing co- and cross-polarized gain components for antenna models with and without EBG structure, and (c) Ansys HFSS simulated peak gain versus frequency comparing antenna models with and without EBG, demonstrating less than 0.8 dBi gain variation over the 27–28.5 GHz band.

REFERENCES

[1] C. Wang, X. You, X. Gao, X. Zhu, Z. Li, C. Zhang, H. Wang, Y. Huang, Y. Chen, H. Haas, J. S. Thompson, E. G. Larsson, M. D. Renzo, W. Tong, P. Zhu, X. Shen, H. V. Poor, and L. Hanzo, "On the road to 6g: Visions, requirements, key technologies, and testbeds," in *IEEE Communications Surveys and Tutorials*, 2023.

[2] G. Lan, Z. Liu, Y. Zhang, T. Scargill, J. Stojkovic, C. Joe-Wong, and M. Gorlatova, "Edge-assisted collaborative image recognition for mobile augmented reality," in *ACM Transactions on Sensor Networks*, 2021.

[3] A. Sabharwal, P. Schniter, D. Guo, D. W. Bliss, S. Rangarajan, and R. Wichman, "In-band full-duplex wireless: Challenges and opportunities," in *IEEE Journal on Selected Areas in Communications*, 2014.

[4] F. Yang and Y. Rahmat-Samii, "Microstrip antennas integrated with electromagnetic band-gap (EBG) structures: A low mutual coupling design for array applications," in *IEEE Transactions on Antennas and Propagation*, 2003.

[5] S. Dey, S. Dey, and S. K. Koul, "Isolation improvement of MIMO antenna using novel EBG and hair-pin shaped DGS at 5G millimeter wave band," in *IEEE Access*, 2021.

[6] S. Ghosh, T. Tran, and T. Le-Ngoc, "Dual-layer EBG-based miniaturized multi-element antenna for MIMO systems," in *IEEE Transactions on Antennas and Propagation*, 2014.

[7] H. S. Farahani, M. Veysi, M. Kamyab, and A. Tadjalli, "Mutual coupling reduction in patch antenna arrays using a UC-EBG superstrate," in *IEEE Antennas and Wireless Propagation Letters*, 2010.

[8] A. K. Oladeinde, E. Aryafar, and B. Pejcinovic, "Mmwave Tx-Rx self-interference suppression through a high impedance surface stacked EBG," in *MDPI Electronics*, 2024.

[9] M. A. Moharram Hassan and A. Kishk, "Bandwidth study of the stacked mushroom EBG unit cells," in *IEEE Transactions on Antennas and Propagation*, 2017.

[10] A. K. Oladeinde, E. Aryafar, and B. Pejcinovic, "EBG placement optimization in a via-fed stacked patch antenna for full-duplex wireless," in *IEEE-APS Topical Conference on Antennas and Propagation in Wireless Communications (APWC)*, 2022.

[11] T. Jiao, T. Jiang, and Y. Li, "Antenna array coupling reduction based on stacked EBG structures," in *International Applied Computational Electromagnetics Society Symposium (ACES)*, 2017.